54. IWK

Internationales Wissenschaftliches Kolloquium
International Scientific Colloquium

Information Technology and Electrical Engineering - Devices and Systems, Materials and Technologies for the Future

Faculty of Electrical Engineering and Information Technology

Startseite / Index:
http://www.db-thueringen.de/servlets/DocumentServlet?id=14089

TECHNISCHE UNIVERSITÄT
ILMENAU

Impressum

Herausgeber: Der Rektor der Technischen Universität Ilmenau
Univ.-Prof. Dr. rer. nat. habil. Dr. h. c. Prof. h. c.
Peter Scharff

Redaktion: Referat Marketing
Andrea Schneider

Fakultät für Elektrotechnik und Informationstechnik
Univ.-Prof. Dr.-Ing. Frank Berger

Redaktionsschluss: 17. August 2009

Technische Realisierung (USB-Flash-Ausgabe):
Institut für Medientechnik an der TU Ilmenau
Dipl.-Ing. Christian Weigel
Dipl.-Ing. Helge Drumm

Technische Realisierung (Online-Ausgabe):
Universitätsbibliothek Ilmenau
ilmedia
Postfach 10 05 65
98684 Ilmenau

Verlag:
Verlag ISLE, Betriebsstätte des ISLE e.V.
Werner-von-Siemens-Str. 16
98693 Ilmenau

ISBN (USB-Flash-Ausgabe): 978-3-938843-45-1
ISBN (Druckausgabe der Kurzfassungen): 978-3-938843-44-4

Startseite / Index:
http://www.db-thueringen.de/servlets/DocumentServlet?id=14089

ULTRA-WIDEBAND PSEUDO-NOISE SENSORS AND THEIR APPLICATION IN MEDICAL ENGINEERING, NON-DESTRUCTIVE TESTING AND FOR SEARCH AND RESCUE

J. Sachs[1], F. Bonitz[1], M. Kmec[1], M. Helbig[1], R. Herrmann[1], K. Schilling[1], P. Rauschenbach[2], E. Zaikov[1]

[1]Technische Universität Ilmenau, POB 10 05 65, 98684 Ilmenau, Germany
[2]MEODAT GmbH, Werner-von-Siemens-Str. 3, 98693 Ilmenau, Germany

ABSTRACT

Ultra-Wideband sensing provides new and interesting options for testing and inspection in many different fields. The article deals with a wide spread of different applications. The advantage of UWB-sensing results from the good penetration of the sounding waves through the material under test and its high spatial resolution. A flexible UWB-sensor conception will be discussed. Its working principle is based on pseudo-random sounding waves. The examples considered shall indicate the device performance for quite different sensor tasks.

Index Terms **–** ultra wideband sensor, ultra wideband radar, PN-code, non-destructive testing, trough wall imaging, cancer detection

1. INTRODUCTION

The exploitation of the interaction of electromagnetic waves with matter provides interesting options to gain information from a great deal of different scenarios. To mention only a few, it enables to assess the state of building materials and constructions, to investigate biological tissue, to detect persons buried by rubble after an earthquake or unauthorised people hidden behind walls and many more. The advantage of such methods consists in their non-destructive and continuously running measurement procedure which may work at high speed and in contactless fashion.

Recently, new developments in RF-electronics and the availability of powerful numerical processors at reasonable prices make this sensing approach more and more attractive also for volume applications outside the laboratory.

Depending on the actual tasks, the requirements on the sensing system may be quite different, such as the optimum operational frequency band, measurement speed, sensitivity, system costs, reliability, etc. Also the hard- and software of the sensor devices may be quite different depending on the application.

Sensors applying electromagnetic interactions with the test object have been in use for a long time. But most of such sensors are restricted to a relative narrow bandwidth and consequently they can provide only a small amount of information about the test object. Ultra-wideband sensors may be able to provide more information and by such reduce ambiguities which are inherently part of indirect measurement methods such as electromagnetic sensing.

The article deals with a flexible sensor conception, some performance-figures of UWB-devices and a couple of measurement examples from different fields of application.

2. FLEXIBLE SENSOR CONCEPTION

The idea behind an UWB-sensor is quite different compared with the classical sensor approach where the sensor/transducer simply transforms a given physical value into another value which can easily be captured (e.g. a voltage). In contrast to that, the basic functioning of an UWB-sensor can be divided into two steps:

1. Capturing the interaction of the target (test object or scenario under test) with an electromagnetic field of a large bandwidth.
2. Extracting the wanted information about the target hidden in the measured data.

This conception leads to a generic structure of UWB-sensor devices as depicted in Figure 1. The applicator provides the electromagnetic interface to the test object and fixes size and shape of the volume of interaction. There are various applicators in use:

- *Open coaxial line* touching a material under test: It leads to a small point-shaped test volume
- (unshielded) *probe cable* covered by the material under test: It results in a line-shaped test volume.
- *Antenna*: It causes a cone-shaped or omni-directional test volume depending on antenna radiation characteristics.
- Applicator *array*: If a larger or a complex scenario must be observed, spatially distributed sensors can be beneficial. Such an arrangement requires multi-channel electronics.

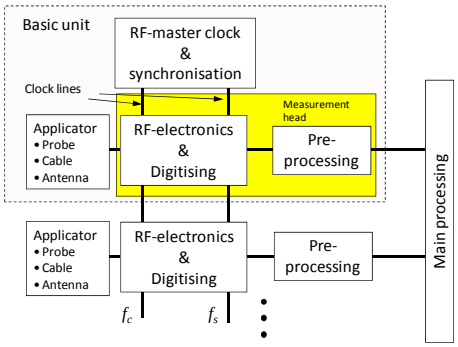

Figure 1: Generic structure of a PN-sequence multi-channel UWB-sensor system

The RF-electronics provide the stimulus signal and capture the target response, which is digitally pre-processed by the following stages. Their basic task and functioning is largely independent from the type of applicator and from the specific application.
Finally, the wanted information is gained by more or less complicated main signal processing. Only in some cases, the processing is so simple that it can be performed by the basic unit itself. The data processing covers mostly application specific tasks of an UWB-sensor. Its complexity largely depends on the actual measurement task and the wanted results (e.g. processing in the time or frequency domain; providing measurement curves or 2D/3D images; feature extraction; object recognition etc.), the user interface, the required refresh rate of the measurements, the control mechanisms of larger sensor arrays, and many things more. Due to its high specificity, we will not consider this aspect in this paper.

3. BASIC FUNCTION PRINCIPLE

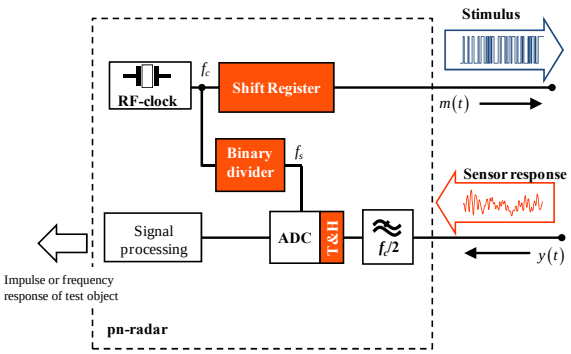

Figure2: Basic concept of the PN-sensor. Note, the measured impulse response function g(t) results from the behaviour of the antennas, of the target and the propagation path.

The basic principle of function of the ultra-wideband PN-sequence approach was introduced in [1]. Figure 2 illustrates the key components. The general idea is to stimulate the scenario under test by a wideband signal which distributes its energy over a large time. This avoids voltages peaks which prevent the electronics and sensible targets from saturation or even damage.
This stimulus signal is provided by a digital shift register. Such a register consists of n high speed flip-flops and it is pushed by a stable RF-clock of frequency f_c. Depending on the internal feedbacks, a PN-sequence is periodically generated. One period of such a signal consists of $N = 2^n$-1 randomly distributed elementary pulses (or chips). Here, we only consider the so called M-sequence. But the approach is not restricted to that specific PN-code. Gold-codes, Kasami-codes or any other code is also applicable as long as it covers 2^n-1 (or 2^n+1) chips per period. The output of the shift register is directly used as stimulus for an antenna/applicator or other measurement object.
The receive signal which represents the response of the test object with respect to the PN-sequence stimulation is immediately sampled via a wideband T&H- or S&H-circuit and converted into the numerical domain by a video-ADC. The signal recording works in a sub-sampling mode in order to reduce the sampling rate. It is controlled by a binary divider.
The acquired data are processed according the actual needs by a FPGA, DSP or by a PC.
In order to gain time resolution for e.g. radar measurements, the measurement signal must be compressed in the receiver which may be carried out by correlation. This finally leads to the wanted impulse response function of the scenario under test. The correlation is executed numerically so that the resulting correlation peaks do not stress analog electronic components.
In the case that the frequency response function is wanted as measurement result, the captured data has to be subjected to a Fourier transform and subsequent processing in the frequency domain.
In all of our applications so far, the PN sounding signal was an M-sequence since it provides the best range resolution as well as a flat stimulus spectrum and it leads to the fastest signal processing. Figure 3 summarises some properties of M-sequences. For reasons of space, only a short sequence is demonstrated. The period length T_0 depends from the shift register length n and the clock rate f_c. The auto-correlation function represents a comb of sharp triangular spikes. Their base width is identical with the length of two chips. Range resolution and ambiguity range of a radar sensor results from the properties of the auto-correlation function (see below). The power spectrum of the M-sequence is a line spectrum having a sinc²-shaped envelope. Theoretically the M-sequence has an infinite wide spectrum. However about 80 % of signal power is concentrated between DC and $f_c/2$. Hence, cutting the spectrum at $f_c/2$ will not drastically degrade the signal properties. In contrary, the band limitation will cut-out a spectral band in which noise and interference increasingly dominate over the signal. This is the

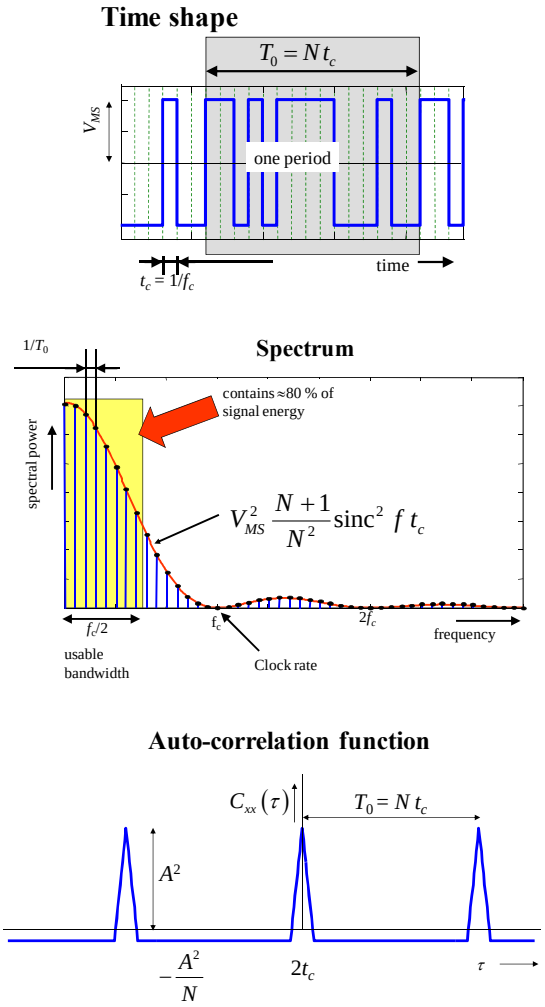

Figure 3: Time shape, spectrum (linear scaled magnitude) and auto-correlation function of a 4th order M-sequence.

reason for the low-pass filter at the receiver input in Figure 2.

A second aspect – a point of central importance – of that band limitation relates to the Nyquist-theorem. If the stimulus bandwidth is limited to $f_c/2$, the lowest possible sampling rate equals the clock rate f_c of the shift register.This has two consequences.

First, the amount of data per measured impulse or frequency response function corresponds to the theoretical minimum. The data throughput of the ultra-wideband sensor may be enormous. Therefore, any redundancy should be avoided during the data capturing. The visualisation of such an impulse response is not always friendly for the human eyes due to the big steps between adjacent data samples. If so, interpolation (preferably by a FFT-approach) improves the appearance of the measurement curves.

Second, sampling with the clock rate f_c means that one has to take one data sample from every chip of the M-sequence. Since the M-sequence is periodic, one can distribute the data gathering over several periods which leads to relaxed speed requirements for the data capturing system. This is a usual approach for RF-signal capturing which is called sub-sampling or stroboscopic sampling.

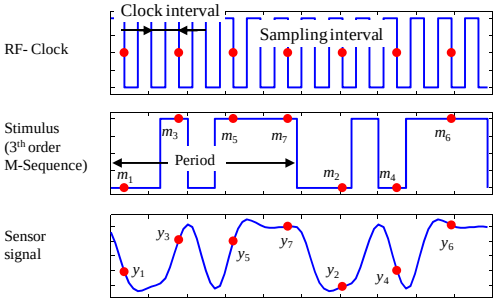

Figure 4: Sub-sampling (stroboscopic sampling) control by binary divider.

The particularity in this case is that the sub-sampling can be controlled by a binary divider due to the fact that the M-sequence (or another PN-code) has a length which is always one less than a power of two $N = 2^n - 1$. Figure 4 demonstrates why. Let us suppose a sampling rate of half the clock rate $f_s = f_c/2$. Therefore only every second chip is sampled. Within the first signal period these are the samples with an odd number and during the second period the samples with the even numbers are captured. The next period will be again the turn for the odd sample numbers and then the even sample numbers will follow and so forth. So after two periods, all data samples are captured without violation of the Nyquist theorem. The same holds for a dividing factor of 4, 8, etc. requiring 4, 8, etc. periods to capture the complete data set for one impulse or frequency response function.

Compared to the usual sampling control in sampling scopes (slow and fast voltage ramps), this method is extremely stable. The divider has to run through all his states before he releases a new sampling event. Thus, differences in the behaviour of the flip-flops in the divider cannot cause variations of the sampling interval. An equidistant and known sampling interval is an important prerequisite to perform a distortion free Fourier-transform.

Furthermore, in order to define trigger events (as e.g. the release of a voltage sample), usually a reference waveform crosses a threshold as depicted in Figure 5. Unfortunately, neither reference signal nor threshold are ideal. They are affected by noise and drift leading to random (jitter) and slow (drift) fluctuations of the trigger point. Obviously these perturbations have less impact as shorter the rise time t_r of the reference waveform becomes smaller. In our case, for the principle demonstrated in Figure 2, the rise time is given by the switching time of the flip-flops which is in the order of 20 ps. Hence, drift and jitter are orders below that of classical sub-sampling devices. A drift free data capturing is important for the application of calibration techniques, since the calibration cannot be

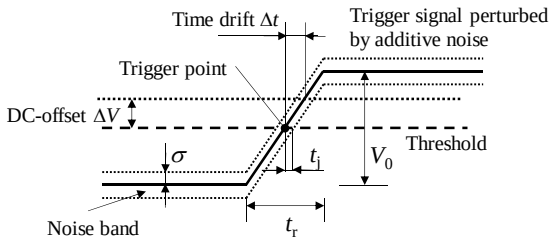

rms-jitter: $\Delta t \approx t_r \, \Delta V / V_0$

drift: $t_j \approx t_r \, \sigma / V_0$

Figure 5: Generation of jitter and drift by additive noise and dc-offset

repeated very often. A jitter free gathering of data results in a high sensitivity to detect small variations within a test scenario.

In order to present the measurement data in a useful form, some processing must be undertaken. Depending on the application, either a frequency response or an impulse response function is of interest. The frequency response is gained via a Fourier transform and the determination of the impulse response requires a time compression of the data. In what follows, we will concentrate on the last point since it is more unusual as the Fourier transform and hence it needs further explanations.

The wanted impulse response function $g(t)$ relates to the input and output signals by

$$\psi_{ym}(\tau) = g(\tau) * \psi_{mm}(\tau)$$

in which $\psi_{mm}(\tau)$ is the auto-correlation of the transmit signal, $\psi_{ym}(\tau)$ is the cross correlation between receive and transmit signal and $*$ symbolises convolution. If the bandwidth of the test signal is large compared to that of the scenario under test, $\psi_{mm}(\tau)$ is short versus any variations in $g(\tau)$ and the equation may be simplified to $\psi_{ym}(\tau) \sim g(\tau)$ for $\psi_{mm}(\tau) \approx \delta(\tau)$. Hence, the input-output-correlation gives the wanted characteristic function of the measurement scenario. The cross-correlation is defined by

$$\psi_{ym}(\tau) = \int y(t) \cdot m(t+\tau) \, \mathrm{d}t \, .$$

For sampled data $\mathbf{m} = [m_1 \quad m_2 \quad m_3 \quad \cdots \quad m_N]^T$ and $\mathbf{y} = [y_1 \quad y_2 \quad y_3 \quad \cdots \quad y_N]^T$, it can be expressed by a matrix equation as long as the settling time of the scenario is shorter than the period length of the PN-code:

$$\begin{bmatrix} \psi_{ym,1} \\ \psi_{ym,2} \\ \psi_{ym,3} \\ \vdots \\ \psi_{ym,N} \end{bmatrix} = \begin{bmatrix} m_1 & m_2 & m_3 & \cdots & m_N \\ m_N & m_1 & m_2 & \cdots & m_{N-1} \\ m_{N-1} & m_N & m_1 & \cdots & m_{N-2} \\ \vdots & \vdots & \vdots & \ddots & \vdots \\ m_2 & m_3 & m_4 & \cdots & m_1 \end{bmatrix} \cdot \begin{bmatrix} y_1 \\ y_2 \\ y_3 \\ \vdots \\ y_N \end{bmatrix}$$

$$\boldsymbol{\psi}_{ym} = \mathbf{M} \cdot \mathbf{y} \sim \mathbf{g}$$

This equation represents a cyclic correlation in which the (NxN) matrix **M** is built from shifted versions of the digitised transmitter signal **m**. **g** is the digitised version of the wanted impulse response function.

Up to now, **m** may represent one period of any wideband signal. It must not be a PN-sequence. However, if the transmit signal is an M-sequence, the matrix **M** can be decomposed in a Hadamard-matrix $\mathbf{M} = \mathbf{P} \cdot \mathbf{H} \cdot \mathbf{Q}$ [2]. Thus, the correlation is expressed as

$$\boldsymbol{\psi}_{ym} = \mathbf{P} \cdot \mathbf{H} \cdot \mathbf{Q} \cdot \mathbf{y} \, .$$

Here, **H** is the [(N+1)x(N+1)] Hadamard matrix, **P** and **Q** are permutation matrices of order [Nx(N+1)] respectively[(N+1)xN)]. The permutation matrices have in maximum only one 1 per row and column. The remaining elements are zeros. Hence, the product of a permutation matrix with a vector represents simply a restructuring of the element order in that vector. Numerically, this is a simple and fast algorithm. Consequently, the correlation consists of three steps:

- Permute the elements of the measured data **y** corresponding to **Q**.
- Perform the product with the Hadamard matrix.
- Permute the elements of the matrix product corresponding to **P**.

A matrix multiplication is usually a numerical expensive procedure. But it is not true for the Hadamard matrix. Here, the matrix product is reduced to $n2^n$ summations which can be calculated in a very fast way which is also referred as Fast Hadamard Transform (FHT). This is depicted in Figure 6 for two simple examples.

In summary, the options to pre-process the measurement data are:

- Subject the captured data to an FFT. This results in a complex spectrum roughly proportional to the frequency behaviour of the transmission path.
- Subject the captured data to an FHT. This leads to the impulse response which is based on the assumption of system stimulation by an ideal M-sequence.
- Measure both, stimulus and system reaction, and calculate the actual cyclic cross-correlation. This leads to the impulse response of the object under test.

- Measure both, stimulus and system reaction, and calculate the complex cross-spectrum via FFT. The result is the frequency response function of the tested system.

$$\mathbf{H}_2 \cdot \mathbf{A} = \begin{bmatrix} 1 & 1 \\ 1 & -1 \end{bmatrix} \cdot \begin{bmatrix} a \\ b \end{bmatrix}$$

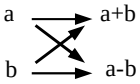

$$\mathbf{H}_4 \cdot \mathbf{A} = \begin{bmatrix} 1 & 1 & 1 & 1 \\ 1 & -1 & 1 & -1 \\ 1 & 1 & -1 & -1 \\ 1 & -1 & -1 & 1 \end{bmatrix} \cdot \begin{bmatrix} a \\ b \\ c \\ d \end{bmatrix}$$

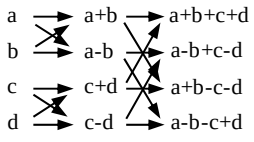

Figure 6: The Hadamard-butterfly which leads to the Fast Hadamard-Transform (FHT)

4. KEY FIGURES

Ambiguity function: The wideband ambiguity function is given by [3]:

$$\chi_{WB}(\tau, s) = \sqrt{|s|} \int_{T_{obs}} m(t)\, y(s(t-\tau))\, \mathrm{d}t$$

with $s = \dfrac{c - v_r}{c + v_r}$

Here, s is a scaling factor which describes the compression or expansion of the scattered waveform by a moving target. For positive radial speed v_r (the target moves away from the antennas), the scaling factor is smaller than one and it is bigger than one if the target approaches. c is the speed of light.

Figure 7 depicts the central peak of the ambiguity function for a short M-sequence which was observed over 128 periods. The ambiguity function is periodic along the range direction restricting the unambiguous range to $R_0 \cong 2^{n-1} c/f_c = N\, t_c/2$. Within the area limited by the -3dB level, the radar is not able to distinguish close targets and the waveform is not sensible to Doppler. The width of this area in range direction denotes the range resolution $\delta_r \approx c\, t_c/2 = c/2\, f_c = R_0/N$, which can be illustrated by the simple model in Figure 7 (bottom). The drawing depicts the limiting case where the compressed waveforms scattered by two targets melt into each other. Note that this simple model refers to the ideal auto-correlation function of the M-sequence which does not respect the frequency cutting at $f_c/2$. Furthermore, the scattered field of a point target is proportional to the second derivation of the incident wave. This is also not included here.

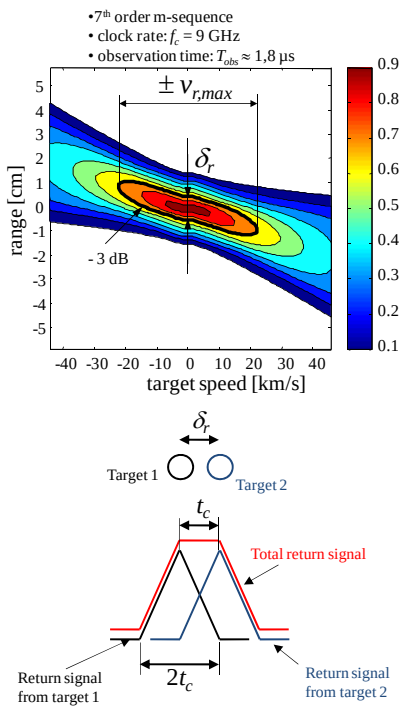

Figure 7: Central peak of the wideband ambiguity function (above) and simplified model to estimate range resolution (bottom).

The speed interval $\pm v_{r,max}$ in which the return signal is not affected by Doppler is given by $|v_{r,\max}| \approx c\, t_c/2\, T_{obs} = \delta_r/T_{obs}$. That is, the target displacement during the measurement time T_{obs} must be less than the range resolution. The observation time is always the multiple of the M-sequence period $T_{obs} = P \cdot T_0$. For the shortest possible measurement time $T_{obs} = T_0$, the maximum "Doppler free" target speed is $|v_{r,\max}| \approx c/2\, N$.

Accuracy: The capability of the radar to register small displacements of the target we call accuracy. The flank of the correlation function will be somewhat shifted if the target moves a bit. But typically only one or a few data samples are located on the flank. Hence, the movement of the flank can only be registered by the voltage variation of these samples. The smallest detectable voltage variation is limited by the noise on the flank. Its variance can be estimated by $\sigma^2_{flank} \approx \sigma^2 + \left(\psi_{ym,\max} \cdot t_j/t_c\right)^2$ (σ^2– variance of ψ_{ym}, t_j – jitter). This finally results in an accuracy of $\Delta r \approx c\, t_c \sigma_{flank}/2\, \psi_{my,max}$ which leads to $\Delta r \approx \delta_r/\sqrt{SNR}$ if the jitter is negligible as in the case of the considered PN-radar (*SNR* – signal to noise ratio).

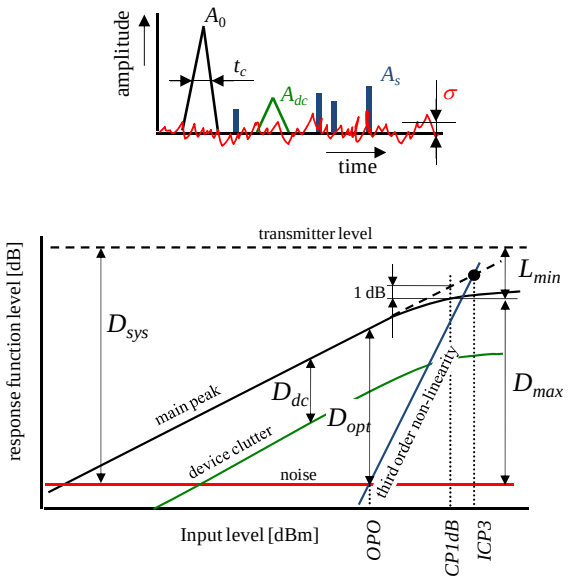

Figure 8: Schematised impulse response (i.e. correlation function) of an idealised wideband transmission path corrupted by several perturbation effects. The level diagram depicts the behaviour of the perturbations in dependence from the input level of the receiver. ***A_0*** *– wanted main peak;* ***A_{dc}*** *– peak of device internal clutter;* ***A_s*** *– spurious signals caused by non-linearity;* ***σ*** *– rms-value of noise.*

Dynamic range: The dynamic range is limited by several effects such as noise, device internal clutter and spurious signal peaks caused by the non-linear behaviour of the receiver. Here, we will only discuss their effect in the time domain i.e. onto the impulse response function. Figure 8 illustrates a short triangular impulse response affected by these perturbations and their dependence from the receiver input level. From that different dynamic ranges can be defined:

Clutter free dynamic range D_{dc}: It is limited by device internal imperfections (reflections, band limitations etc.) and by the deviation of the actual transmitted M-sequence from the ideal one. It can be largely removed by an appropriate calibration [4],[5]. After calibration, D_{dc} is mainly limited by the quality of the calibration standards and the stability of the measurement device over time. The clutter free dynamic range D_{dc} dominates the device performance to detect static objects.

Spurious free dynamic range D_{opt} and optimal point of operation OPO: Non-linear distortions of the received signal cause additional spikes in the correlation function [6]. It has been seen from measurements that the third order non-linearity dominates this effect. The spurious free dynamic range D_{opt} also limits the device performance to detect static objects.

Maximum signal to noise ratio D_{max}: It is given by the relation between maximum signal level (usually the 1 dB compression point) and the noise level. Note, that the value of D_{max} depends on the observation time T_{obs}:

$$D_{\max} = SNR_{\max} = \eta \cdot E / N_p = SNR_0\, \eta \cdot T_{obs} \cdot f_c .$$

Herein are: E the signal energy provided by the measurement object during the observation time T_{obs}, N_p the noise power spectral density, η the receiver efficiency (in our case $\eta = 2^{-m}$); SNR_0 the signal to noise ratio of the captured signal. If SNR_0 is expressed in effective number of bits *ENOB*, D_{max} can be estimated to (assuming an ideal M-sequence)

$$D_{\max}\,[\mathrm{dB}] \approx 4.77 + 6 \cdot ENOB + 3(n-m) + 10 \lg p$$

$$\text{with} \quad p = i \cdot 2^m,\ i = 1, 2, 3, \cdots$$

n and m are the orders of the shift register and binary divider and p is the number of signal periods over which the measurement was done, i.e. $T_{obs} = p \cdot T_0 = i \cdot 2^m \cdot T_0$. The value of i indicates the number of synchronous averaging. D_{max} mainly limits the sensibility to detect weak moving targets since the mostly static device internal clutter and the spurious signals may be removed by appropriate low pass filtering.

System performance D_{sys}: It indicates the weakest propagation path which can be observed by the radar. It results from D_{max} and the attenuation of the strongest signal path L_{min} (usually antenna cross-talk).

5. SOME VARIATIONS OF SYSTEM CONCEPTS

As seen from the previous paragraph, the key figures of the radar system may be flexibly matched to different requirements by selecting f_c, n, m and p. Additional degrees of freedom are given by varying the code of the sounding signal and the type of data processing. Since all fundamental system components are based on digital circuits, a switching between several modes is in principle also possible during operation. The structure of the system may be adapted to many different requirements. Figure 9 summarises some variants which can also be combined.

- *MIMO-System; UWB-array*: In principle an arbitrary number of transmitter and receiver channels can be combined. The receivers are usually all working in parallel. The operational mode of the transmitters must respect the orthogonality of the sounding signals.
- *Increased equivalent sampling rate*: The idea is to capture more than one sample per chip. Therefore, the low-pass filter at the receiver input can be dropped since the band limitation will be carried out inherently by the electronic

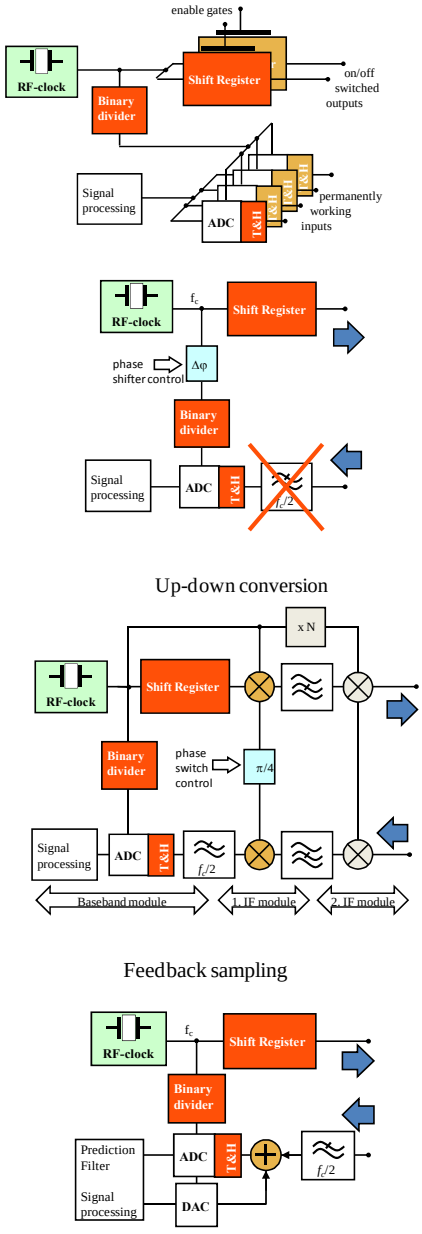

Figure 9: Some of the possible variations of PN-radar device structures.

components. Digital signal processing will then partially take over the noise suppression of that filter. This approach is useful if the clock rate must be changed during operation or to extend the operational frequency band (using a larger bandwidth of the stimulus supposed) [7]-[9].

- *Up-down-conversion*: The operational band can be shifted to an arbitrary band. The up-conversion of the first IF-stage works by a xor-gate and the IQ-down-conversion works sequentially in order to assure identical I- and Q-channels over a huge bandwidth ([9]-[11]).
- *Feedback sampling*: The data variations from measurement to measurement are almost quite small due to the fast measurement speed. This can be used to predict the next expected value and to capture only the difference. Hence, the dynamic range will be increased by avoiding T&H saturation and the load of the digital system is reduced since only low bit values have to be handled.

6. EXAMPLES OF TECHNICAL IMPLEMENTATIONS

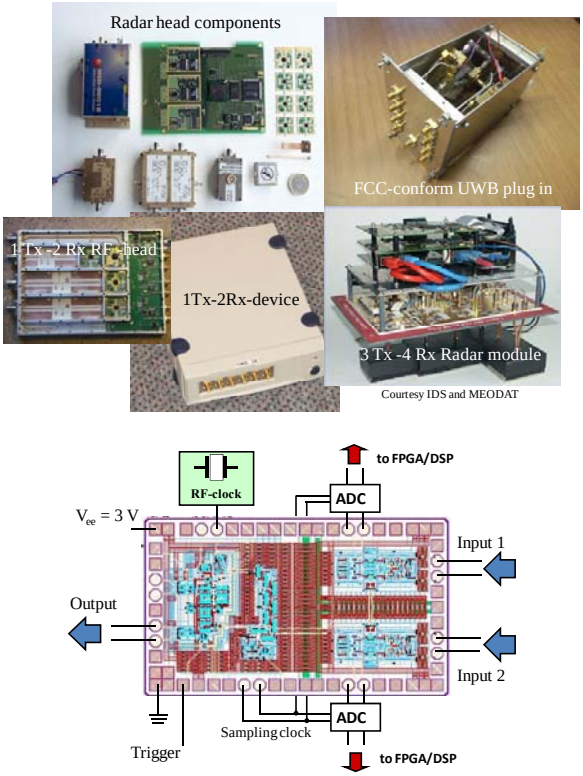

Figure 10: Some basic subcomponents and examples of PN-short range radar system implementations and a new 1Tx-2 Rx single chip radar which is just under investigation.

The technical implementation of the radar device is divided in an RF-part and a digital part. The key-components of the RF-part are custom-made SiGe:C-circuits which can be individually combined to a specific RF-head. Figure 10 gives some examples. The custom ICs are emphasised by the red boxes in the block schematics (Figure 2 and Figure 9). The shift-register lengths used up to now were 9 and 12. The maximum clock rate of the shift register is more than 20 GHz. The analogue band width of the T&H is also about 20 GHz and their maximum sampling rate is about 3 GHz. New developments are directed to completely integrate the RF-part as to be seen in Figure 10 bottom. Currently, the digital part consists of video-ADCs which operate in the 20 MHz-range (depending on the RF-clock rate and the binary divider), a FPGA for data pre-processing and a DSP.

7. APPLICATIONS

So far, the implemented systems and investigated applications were focused on high resolution short range sensing. The following compilation gives a few examples in order to underline the flexibility of the ultra-wideband PN-radar sensor. The table of references lists further research topics in which PN-sensors were involved.

Through wall tracking of people

The penetration of electromagnetic waves through building material is reasonable if their frequency is below 2...3 GHz. This opens up the opportunity to detect reflective targets hidden behind walls. Since nearly all objects reflect electromagnetic waves, the returning waves superimpose to a complicated mixture of signals. The simplest way to extract meaningful signal components from this tangle of waves is to consider only non stationary objects such as e.g. walking people and to extract their roundtrip time. The target localisation is based on an interferometric radar approach and tri-lateration as illustrated in Figure 11.

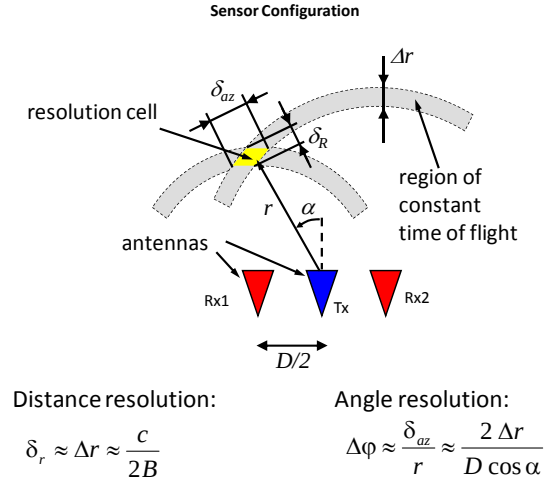

Figure 11: Principle of localisation of moving target by tri-lateration and illustration of sensor use.

The visualisation of large stationary targets behind a wall is possible too. But it requires scanning and sophisticated radar imaging [19]–[22]. For further examples of ultra-wideband localisation and tracking, the reader is conducted to [23]-[25].

Breathing detection through rubble

The rescue of buried people which are still alive after an earth quake is a crucial task. The most demanding issue relates to a fast detection of the victims. But since many of the victims are trapped or unconscious, they are not able to attract attention to themselves. Here, a sensor which is able to register breathing people may save valuable time. Ultra-wideband sensors can do this job by registering the small movement of the human chest due to breathing.
The rubble is often mixed with reinforced concrete. It provides huge clutter signals from which the weak "breathing signals" must be extracted by a sophisticated signal processing [26]. Figure 12 illustrates an example. It indicates the detection of a victim having a breathing interval of a bit less than 3 seconds. The time scale on the vertical axis relates to the roundtrip time of the sounding waves. Using more than one antenna, such measurements can be used to localise the target.

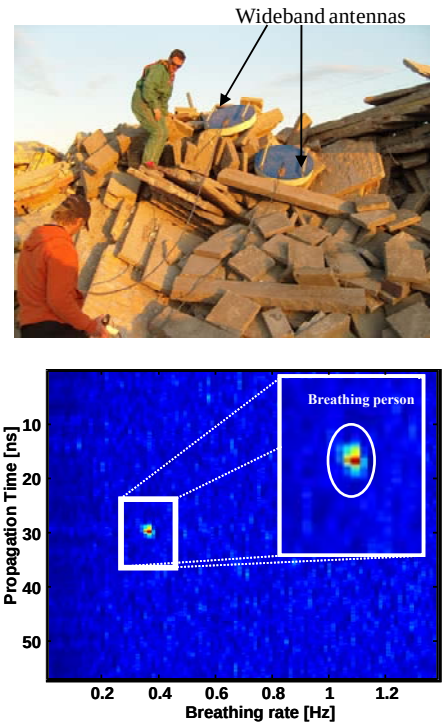

Figure 12: Search for a buried people by ultra-wideband radar and visualisation of processed data.

Medical applications

In the environment of medical engineering, the use of ultra-wideband sensor can address several fields of applications as e.g. remote sensing of vital data [27] or the fusion of multi-modal sensor arrangements [28], [29]. Here, we will discuss a further use which is based on moisture sensing. Water is one of the most important substances of life. The water molecule shows a specific behaviour in the electric field [30]. It has a very high permittivity at frequencies below 1

GHz and shows relaxation phenomena in the lower microwave rage. This behaviour makes water very interesting for ultra-wideband sensing.
Because the state of biological tissue largely depends on its water content, ultra wideband sensing of tissue may be an interesting alternative to existing methods in the future. So, e.g., the water quantity is enhanced in many types of cancerous tissues compared to healthy human cells. This opens up the opportunity to search for cancer by harmless electromagnetic sensing. Figure 13 represents an example of a cancerous lunge which was scanned by a coaxial probe in order to gain its frequency dependent complex permittivity. From that the water content was calculated via an appropriate model [31], [32]. As the investigation shows, the water content of the tissue clearly rises by approaching the cancerous regions.

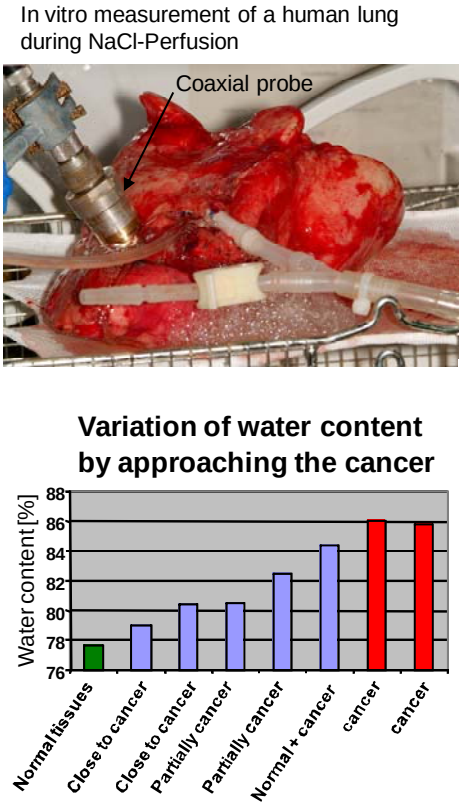

Figure 13: Screening of a cancerous lung by dielectric spectroscopy using a coaxial probe. The measurements were performed with an M-sequence device of 4 GHz bandwidth (Courtesy Universitätsklinikum Heidelberg, Experimentelle Chirurgie).

High resolution radar imaging

The short pulse width respectively the short coherence length of ultra-wideband signals is the prerequisite to calculate high resolution radar images from captured signals. Since the sounding waves can penetrate many substances, these images may also map hidden objects.

Radar imaging requires data capturing from different aspect angles referred to the object of interest. Three basic approaches are in use for that purpose [33]:

- A great deal of radar sensors is spread over a large area. The arrangement of the sensors may be regular or arbitrary as well as dense or sparse (it is called physical array - PAR)
- A single sensor is moved across an area of interest while the radar data are coherently captured (this is called synthetic array- SAR)
- A stationary single sensor captures the radar returns from a moving object (this is called inverse synthetic aperture – ISAR).

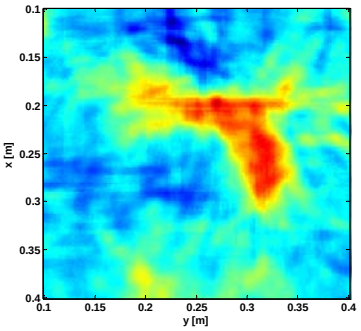

Figure 14: Radar image of a hand gun gained from migration imaging of SAR-data. The operational frequency of the radar device covers the band 1 to 3.5 GHz.

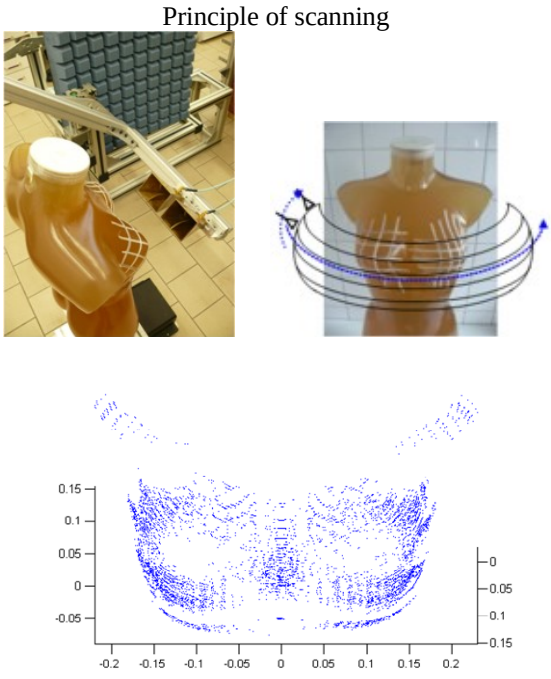

Figure 15: 3D-breast surface reconstruction of a body surrogate aimed at medical purposes. The imaging is based on Inverse Boundary Scattering Transform using M-sequence radar (1-13 GHz frequency band) for data collection.

The processing of the captured data is usually performed by migration [22]. The corresponding algorithms are either based on space-time procedures (e.g. Kirchhoff migration) or they are dealing with Fourier transformed data i.e. frequency-wave number procedures (e.g. Stolt migration [34]). Newer approaches apply Inverse Boundary Scattering Transform [35]- [38]. They provide better results as the migration. However, the surfaces of the objects should be sufficiently smooth and it should be possible to extract the fronts of the scattered wave from the captured signals. The figures above show examples of a migrated radar image and the 3D-reconstruction of a body surrogate which is intended as an intermediate state of breast cancer detection.

Non-destructive testing in civil engineering

Non-destructive testing in civil engineering covers a wide field of different applications which are spanned from investigations for underground and mine work to tests in structural engineering as well as for material and pavement characterisation. The following figures illustrate some corresponding examples.

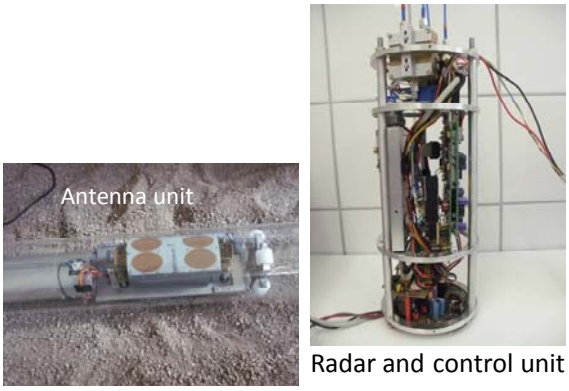

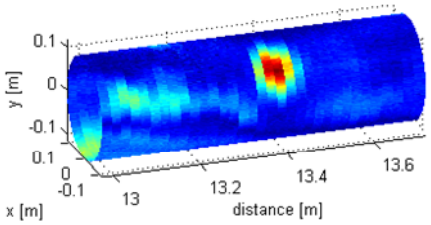

Figure 16: Radar tube crawler intended for quality assurance of waste tube embedding. The radar image shows a foreign body close the tube cladding which may be the cause of long term damages.

Figure 16 refers to investigations of the embedding zone of waste water tubes. The quality and state of that zone largely determines the live time of the tubes [39], [40].

The damage of the crystalline structure of salt rock in mines is shown in Figure.17. It is visualised from the

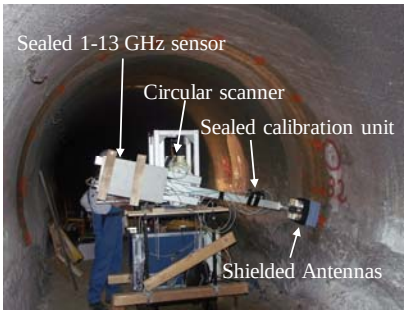

Visualisation of structural defects

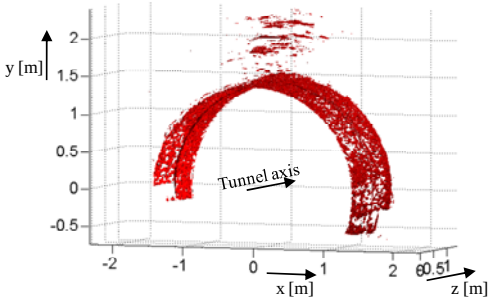

Figure 17: Salt mine inspection with ultra-wideband radar. The lower image emphasizes the sources of back scattering which are caused by the structural defects in the salt.

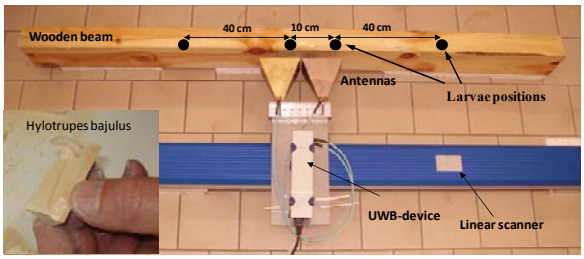

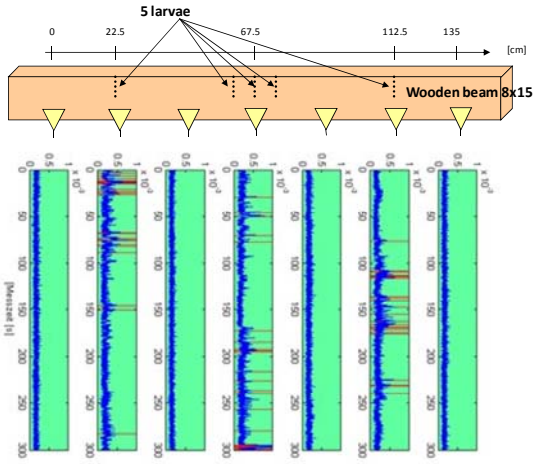

Figure 18: Detection of wooden worms due to their feed movement.

weak back scattering of very wideband waves (1...13 GHz) due to these structure defects [4], [5]. For deeper details on the examples from Figure 16 and 17, the reader is addressed to [41] which are to be found

in this proceeding too. Finally, Figure 18 demonstrates the use of ultra-wideband sensors for the detection of wood-destructible insects [42]. The marginal movement of the larvae provide evidence of their existence. A larva contains more water than the surrounding wood. Hence, it provokes a weak reflection of electromagnetic waves which can be distinguished from other reflection if the larva slightly moves.

8. SUMMARY

Ultra-wideband sensing represents an interesting and innovative sensing tool with a large area of applications. It is based on the interaction of harmless low-power microwaves with the objects of interest. This sensing method permits the continuous, contactless and non-destructive characterisation of the measurement objects. The article has shown some application examples from different areas. Further examples can be found in the proceedings of the biannual GPR conferences.
The functioning of ultra-wideband sensors may be based on different approaches. Here, we considered the use of very wideband pseudo-noise signals. It promotes a very stable and hence sensible sensor electronics which can be monolithically integrated in a low-cost RF-technology.

9. ACKNOWLEDGMENT

The authors appreciate the support by European (e.g. Demine, Demand, Radiotect, Pulsers I-II) and national projects (e.g. 2C1194, 16IN0338, SA 1035/2-1; SA 1035/3-1; SA 1035/4-1) and we are grateful for the help and assistance of all our cooperation partners.

10. REFERENCES

[1] J. Sachs, P. Peyerl, and M. Roßberg, “A New Principle for Sensor-Array-Application.,” in IEEE Instrumentation and Measurement Technology (IMTC), Venice (Italy), pp. 1390-1395, 1999.

[2] N. Xiang, "A Mobile Universal Measuring System for the Binaural Room-Acoustic Modelling-Technique," Bundesanstalt für Arbeitsschutz, 1991.

[3] L. G. Weiss, “Wavelets and Wideband Correlation Processing,” IEEE Signal Processing Magazine, pp. 19, January, 1994.

[4] [R. Herrmann, J. Sachs, and P. Peyerl, “System evaluation of an M-sequence ultra wideband radar for crack detection in salt rock,” in International Conference on Ground Penetrating Radars (GPR), Ohio (Columbus), 2006.

[5] R. Herrmann, J. Sachs, K. Schilling et al., “12-GHz Bandwidth M-Sequence Radar for Crack Detection and High Resolution Imaging,” in International Conference on Ground Penetrating Radar (GPR), Birmingham, UK, 2008.

[6] H. Alrutz, “Über die Anwendung von Pseudorauschfolgen zur Messung an linearen Übertragungssystemen,” Thesis, Mathematisch-Naturwissenschaftliche Fachbereiche, Georg-August-Universität zu Göttingen, Göttingen, 1983.

[7] J. Sachs, R. Herrmann, M. Kmec et al., “Modified M-Sequence UWB-Radar,” in German Microwave Conference (GeMic), Karlsruhe (Germany), 2006.

[8] J. Sachs, R. Herrmann, M. Kmec et al., “Recent Advances and Applications of M-Sequence based Ultra-Wideband Sensors,” in International Conference on Ultra-Wideband, Singapore, 2007.

[9] M. Kmec, R. Herrmann, J. Sachs et al., "Extended Approaches for M-Sequence based UWB systems.," In Ultra-Wideband, Short-Pulse Electromagnetics 8, C. E. Baum, A. P. Stone and J. S. Tyo, eds., pp. 135-142: Springer, 2007.

[10] J. Sachs, M. Kmec, R. Zetik et al., “MSCW-Radar – a Novel Ultra Wideband Radar Principle,” in International Radar Symposium (IRS), Berlin (Germany), 2005.

[11] M. Kmec, J. Müller, P. Rauschenbach et al., “Integrated cm - and mm-Wave UWB Transceiver for M-Sequence Based Sensors,” in European Electromagnetics (EUROEM), Lausanne (Switzerland), 2008.

[12] R. Zetik, S. Crabbe, J. Krajnak et al., “Detection and localization of persons behind obstacles using M-sequence through-the wall radar,” in SPIE Defense & Security Symposium, Orlando (Florida), 2006.

[13] R. Zetik, J. Sachs, and P. Peyerl, "Through-Wall Imaging by Means of UWB Radar," Short-Pulse Electromagnetics 7, F. Sabath, E. L. Mokole, U. Schenk et al., eds., pp. 613-622: Springer, 2007.

[14] N. T. Thành, L. v. Kempen, T. G. Savelyev et al., “Comparison of basic inversion techniques for through-wall imaging using UWB radar,” in European Radar Conference (EURAD), Amsterdam (The Netherlands), 2008.

[15] J. Sachs, M. Aftanas, S. Crabbe et al., “Detection and Tracking of Moving or Trapped People Hidden by Obstacles using Ultra-Wideband Pseudo-Noise

Radar," in European Radar Conference (EURAD 2008), Amsterdam (The Netherlands), 2008.

[16] J. Rovnakova, M. Svecova, D. Kocur, T.T. Nguyen, J. Sachs, "Signal Processing for Through Wall Moving Target Tracking by M-sequence UWB Radar," The 18th International Conference Radioelektronika, pp. 65-68., Prague, Czech Republic, 2008.

[17] J. Rovnakova, "Compensation of Wall Effect for Through Wall Moving Target Localization by UWB Radar," The 8th Scientific Conference of Young Researchers, Kosice, 2008.

[18] J. Rovnakova, "Complete Signal Processing Procedure for Through Wall Target Tracking: Description and Evaluation on Real Radar Data," The 9th Scientific Conference of Young Researchers, accepted for publication, Kosice, 2009.

[19] M. Aftanas, J. Rovnakova, M. Drutarovsky, and D. Kocur, "Efficient Method of TOA Estimation for Through Wall Imaging by UWB Radar," IEEE International Conference on Ultra-Wideband (ICUWB2008), vol. 10, pp. 101–104, Sept. 2008.

[20] M. Aftanas, "Signal Processing Steps for Objects Imaging Through the Wall with UWB Radar," 9th Scientific Conference of Young Researchers, SCYR 2009, Faculty of Electrical Engineering and Informatics, Technical University of Košice, Slovak Republic, May 2009.

[21] M. Aftanas, M. Drutarovský, "Imaging of the Building Contours with Through the Wall UWB Radar System," Radioengineering, Czech Republic, 2009.

[22] N.T. Thanh, L. van Kempen, T.G. Savelyev, X. Zhuge, M. Aftanas, E. Zaikov, M. Drutarovsky, H. Sahli, "Comparison of Basic Inversion Techniques for Through-Wall Imaging Using UWB Radar," 5th European Radar Conference, EuRAD 2008, Amsterdam, Netherlands, Oct. 2008.

[23] J. Sachs, R. Zetik, P. Peyerl et al., "Autonomous Orientation by Ultra Wideband Sounding," in International Conference on Electromagnetics in Advanced Applications (ICEAA), Torino (Italy), 2005.

[24] D. Porcino, J. Sachs, R. Zetik et al., "UWB Ranging," UWB Communication Systems a comprehensive Overview, M. G. d. Benedetto, T. Kaiser, A. Molisch et al., eds., pp. 411-446: Hindawi Publishing Corporation, 2006.

[25] R. Zetik, J. Sachs, and R. Thomä, "UWB Short Range Radar Sensing -The Architecture of a Baseband, Pseudo-Noise UWB Radar Sensor," Instrumentation & Measurement Magazine, vol. 10, no. April, pp. 39-45, 2007.

[26] E. Zaikov, J. Sachs, M. Aftanas et al., "Detection of trapped people by UWB radar," in German Microwave Conference (GeMiC 2008), Hamburg (Germany), 2008.

[27] J. Sachs, R. Zetik, M. Helbig, E. Zaikov, "Capturing Vital Data by Ultra-Wideband Sensors: An Overview," ARCS 2008, February 25-28, Dresden, Germany, 2008.

[28] F. Thiel, M. Hein, U. Schwarz, J. Sachs, F. Seifert, "Fusion of magnetic resonance imaging and ultra-wideband-radar for biomedical applications," Proceedings ICUWB 2008, Vol. 1, Hannover, Germany, 10-12 September 2008.

[29] F. Thiel, M. Hein, J. Sachs, U. Schwarz, F. Seifert, "Physiological signatures monitored by ultra-wideband-radar validated by magnetic resonance imaging," Proceedings ICUWB 2008, Vol. 1, Hannover, Germany, 10-12 September2008.

[30] U. Kaatze, "Electromagnetic wave Interactions with Water and Aqueous Solutions," In K. Kupfer (editor): Electromagnetic Aquametry. Springer-Verlag Berlin Heidelberg 2005. ISBN 3-540-22222-7, 2005.

[31] M. Schaefer, K. Nowak, B. Kherad et al., "Monitoring water content of rat lung tissue in vivo using microwave reflectometry," Med. Biol. Eng. Comput., 42, 577-580, 2004.

[32] M. Helbig, J. Sachs, U. Schwarz et al., "Ultrabreitband-Sensorik in der medizinischen Diagnostik," in 41. Jahrestagung der Deutschen Gesellschaft für Biomedizinische Technik (BMT 2007), Aachen (Germany), 2007.

[33] J. Sachs, "High-Resolution Short-Range Microwave Imaging: A short Overview," 1st Algerian German International Conference on New Technologies and their Impact on Society AGICNT 2008, UFA Sétif, Sétif, Algeria, 4 - 7 Mai 2008.

[34] R.H. Stolt, "Migration by fourier transform", Geophysics Vol. 43, pp. 23-48, 1978.

[35] S. Kidera, "High-performance 3-D imaging algorithms or UWB pulse radars," Dissertation, Kyoto University, 2007.

[36] M. Helbig, M. A. Hein, U. Schwarz et al., "Preliminary investigations of chest surface identification algorithms for breast cancer detection," in International Conference on Ultra-Wideband, Hannover (Germany), 2008.

[37] M. Helbig, C. Geyer, M. Hein et al., „A breast surface estimation algorithm for UWB microwave imaging," Proc. EMBEC 2008, Antwerpen, 760-763, 2008.

[38] M. Helbig, C. Geyer, M. Hein, R. Herrmann, I. Hilger, U. Schwarz, J. Sachs, "Improved Breast Surface Identification for UWB Microwave Imaging," World Congress of Medical Physics and Biomedical Engineering, Munich, 2009.

[39] F. Bonitz, M. Eidner, J. Sachs et al., "UWB-Radar Sewer Tube Crawler " in 12th International Conference on Ground Penetrating Radar Birmingham (UK), 2008.

[40] J. Sachs, A. Badstübner, F. Bonitz, M. Eidner, M. Helbig, R. Herrmann, M. Kmec, P. Rauschenbach, H. Solas, "High Resolution Non-Destructive Testing in Civil Engineering by Ultra-Wideband Pseudo-Noise Approaches. Proceedings ICUWB 2008, Vol. 2, Hannover, Germany, 10-12 September 2008.

[41] F. Bonitz, R. Herrmann, M. Eidner, J. Sachs, H.Solas, "Application of Ultra Wideband Radar Sensors for Non-Destructive Testing of Pipe Systems and Salt Mine Tunnels," 54th Internationales Wissenschaftliches Kolloquium; Ilmenau University of Technology; 07 – 11 September 2009.

[42] J. Sachs, M. Helbig, K. Renhak, "Unsichtbares wird sichtbar – Mit Radar den Insekten auf der Spur: Neue Möglichkeiten zum Aufspüren von Insektenaktivitäten," HOBA 2008, Duisburg, Germany, 30-31 October 2008.